Fuel 368 (2024) 131602

Contents lists available at ScienceDirect

Fuel

journal homepage: www.elsevier.com/locate/fuel

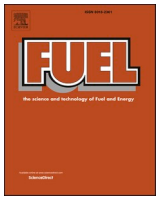

Plasma assisted combustion of different biogas mixtures in low swirl burner

Ernest Bykov *, Adolfas Jančauskas, Rolandas Paulauskas, Kęstutis Zakarauskas, Nerijus Striūgas

Laboratory of Combustion Processes, Lithuanian Energy Institute, Breslaujos str. 3, LT-44403 Kaunas, Lithuania

ARTICLE INFO

Keywords:
Gliding arc
Plasma assisted combustion
Low-swirl-lean burner
Flame chemiluminescence
Low calorific gas

ABSTRACT

This study explores the impact of plasma driving frequency on diverse biogas compositions, emphasizing flame behaviour by analysing spatial emissions of OH*, C_2*, and CH* from plasma-assisted flames. Experimental investigation performed combusting mixtures with 25 % and 60 % CH_4 in CO_2 under lean combustion conditions with the varying fuel equivalence ratios from 0.71 to 0.83 and plasma discharge frequencies from 60 to 120 kHz resulting in higher energy density.

Obtained results indicate that the plasma assistance notably enhances flame stability under lean fuel conditions with increasing frequency from 80 to 120 kHz. The discharge frequency of 60 kHz indicates insufficient energy to enhance combustion of low calorific value mixtures as the flame lift-off height increases approximately by 0.43–1.5 % for the mixture of 25 vol% CH_4 in CO_2 and by 0.26–7.7 % for the mixture of 60 vol% CH_4 in CO_2. Changing the plasma frequency from 80 to 120 kHz, the flame position is shifted closer to the burner nozzle for both mixtures and the highest effect is determined at 120 kHz. The flame lift-off height is reduced by 2.43–16.34 % for the mixture with 25 vol% of CH_4 and by 3.57–51.28 % for the mixture with 60 % of CH_4. The plasma-assisted combustion leads to improved combustion efficiency as CO emissions are reduced from 1550 ppm to 45 ppm for biogas mixture, but in the case of low calorific value gas, the CO emissions increase linearly with the frequency increase even the flame curvature and stability is improved.

1. Introduction

Since the Industrial Revolution, combustion has been the primary method of energy production for various industrial activities, including power generation and transportation [1]. Despite ongoing efforts to enhance combustion efficiency and reduce greenhouse gas emissions (GHG) [2] the reliance on hydrocarbon fuels in these sectors remains a significant contributor to CO_2 emissions, driving global warming and hindering climate change mitigation. Prioritizing decarbonizing the industrial, power generation, and transportation sectors is pivotal for addressing GHG emissions and fulfilling environmental responsibilities. While decarbonisation in the entire fuel sector is a significant goal, its realization is hindered by the widespread use of conventional combustion systems and the need to meet escalating energy demands while minimizing environmental impact [3]. Acknowledging the incremental nature of this process, the European Union initially targeted 32 % renewable energy by 2030, later ambitiously raising the goal to 40 % [4]. Consequently, until a substantial portion of energy demand is met by fully carbon–neutral fuels like NH_3 or H_2, the industry will undergo a "transition" phase, relying on renewable carbon-based fuels to meet energy needs. One such fuel is biogas, known for its methane content that typically ranges from 45 % to 75 % by volume, with most of the remainder being CO_2 [5]. Biogas is a valuable product widely used in various sectors of the national economy, such as energy production, district heating, mobility sector, etc.[6,7] and is also suited as a feedstock for receiving even higher calorific value products. Usually, the calorific value of biogas varies around 21.5 MJ/m^3. In contrast, natural gas is 35.8 MJ/m^3 [8], which leads to the need for the so-called "biogas to biomethane upgrade "process that would allow the gaining of needed higher calorific parameters of the gas after the procedure. In biogas to biomethane upgrade, large volumes of carbon dioxide with a small methane content are generated as an off-gas stream after the methane separation process through the membrane occurs, and the remaining gas is separated. These gases could not be used in some technological or industrial applications due to the challenges connected to high CO_2 content resulting in unstable combustion. While it is hard to use without processing, this gas is mainly utilized on-site or injected back into the primary biogas line to prevent greenhouse gases from escaping to the

* Corresponding author.
E-mail address: ernest.bykov@lei.lt (E. Bykov).

https://doi.org/10.1016/j.fuel.2024.131602
Received 18 October 2023; Received in revised form 22 February 2024; Accepted 24 March 2024
Available online 28 March 2024

atmosphere. Typically, such gas contains about 15–30 % CH_4 and 85–70 % CO_2, which leads to low calorific value of 7–11 MJ/m^3 [9] and are considered as low calorific value (LCV) gases. Such gases require the additional processing for stability and general efficiency improvement of the combustion process. Besides, the instability arising from fluctuations in off-gas composition contributes to undesirable unstable combustion, which holds the potential to harm the combustion system. To avoid emissions to atmosphere, the common method of its utilization is pilot gas combustion [10]. This technique enhances the calorific value of LCV gas through the addition of high calorific value fuel or conducting a two-stage combustion of the incoming reactant. High-calorific-value gases are employed to maintain flame stability when combusting LCV gas–air mixtures. Commonly used gases in pilot gas combustion encompass hydrogen, methane, propane, and similar options [10]. Considering that this method requires the usage of additional fuel leading to higher energy consumptions and increased GHG emissions, other possible method is plasma-assisted combustion, which is gaining more attention for energy production from alternative fuels.

In general, non-thermal plasma is known for its enormous number of different applications: from medical, e.g. non-thermal plasma wound healing [11] to surface improvement applications, e.g. providing antibacterial and self-cleaning properties to polyester/cellulose fabric [12], from CO_2 conversion [13] to pollution control [14]. In the last decade, the plasma-assisted combustion (PAC) is gaining more attention as a method for the combustion and stability enhancement based on the ability of the electrical field to process gases. With the help of energy that this field is carrying by thermal and kinetic mechanism [15], larger molecules can be cracked down into smaller species, which require a lower amount of energy for their oxidation and usage in the combustion process [16]. Combinations of methods of plasma-assisted improvement combustion parameters (raise the calorific value, decrease the induction zone length and also provoke the decrement of the temperature initial ignition parameters [17,18]). Additionally, it is crucial to highlight that non-equilibrium plasma types, such as the Gliding Arc employed in this investigation, exhibit a higher electron temperature ranging from 1 to 10 eV. This characteristic renders them more kinetically active, attributed to the rapid generation of active radicals and excited species through processes like electron impact dissociation, excitation, and subsequent energy relaxation [19,20]. It is noteworthy that many of these electron impact processes display a strong dependence on electron energy. Various types of radicals are known to be significant influencers on the combustion process [21]. Those species produced through gliding arc (GA) plasma are NO*, N_2*, and OH*. Studies have shown variations in their spatial distribution [22]. CH and OH radicals, known as being formatted after the decomposition of hydrocarbons, are some of the biggest influencers on flame stability and temperature because of their oxidative abilities [23,24]. It was also found in the work by Zhu et al. [25] the emission intensity of NO (A-X), OH (A-X) and N_2 (C-B) could increases at high flow rates possibly due to more frequent conversion to the thermal spark-type discharge. As was found by Kim et al.[26], nanosecond repetitively pulsed (NRP) discharges effectively alleviated combustion instability in both dump combustors and model gas turbine combustors, resulting in notable extensions of the lean blowout (LBO) limits. Same behaviour of the plasma influence in the flame blowout limit was observed by Tian Y et al. [27]. The blowout limit increased by 29 % when the GA-type plasma was presenting. In the work [28] discovered that NRP discharges promote the development of a stable inner shear layer, consequently leading to a substantial expansion of the lean blowout limit within a dump combustor featuring axial swirling flows. It was noticed that the blowout limit was extended by approximately 10 % with the increasing discharge repetition rate until saturation. Additionally, in the case of larger-scale burners in the work, Blanchard et al. [29] found that NRP discharges significantly expand the lean blow-off threshold across a broad spectrum of operational conditions, reaching an equivalence ratio as low as 0.16. Demonstrating lean flame stabilization up to 100 kW thermal power, the authors achieved an electric power consumption of less than 0.2 % relative to the flame's thermal power for the plasma assistance process. Furthermore, plasma-assisted lean flames emit lower NOx levels than leanest stable flames without plasma. Exploring diverse pulse patterns instead of continuous discharges at a fixed repetition frequency reduces the plasma-to-flame power ratio required for lean flame stabilization to 0.06 %, further reducing pollutant emissions. Xiong et al. [30] also demonstrated the ability of NRP discharges to stabilize the second-stage chamber in a 50-kW sequential burner using a mere 100 W of plasma power with an insignificant increase in NOx generation. Vignat et al. [31] explored the potential of NRP discharges to enhance the lean blowout (LBO) threshold for liquid fuels. Employing a single swirl-stabilized 5-kW burner at atmospheric pressure, they conducted experiments involving perfectly premixed methane-air and sprays of liquid heptane and liquid dodecane. The results demonstrated a notable expansion of the LBO limit for all three fuels with NRP discharges. This underscores the favourable impact of LBO extension observed in gaseous hydrocarbon mixtures, which can be effectively replicated in spray burner configurations. Finally, in work [32] was found that combining the non-thermal plasma applied burner with a lean-near blow-off combustion process with the help of low swirled (LS) can considerably reduce CO emission compared to those without NTP and with ozone addition only. However, the NTP produces O (10) ppm NOx emission in Regime II, significantly reduced in Regime III near the LBO limit. All results are attributed to the enhanced combustion by streamers or ozone produced by the DBD reactor. To ensure improved combustion, the burner should have a high ability to mix processed gas before it reaches the combustion zone, which obviously leads us to the need for vortex-operated burner usage. Under very lean conditions, the premix flame becomes vulnerable to combustion instability, especially blowout. When the flow rate is high enough, or the mixture equivalence ratio is low enough in the premixed gas combustor, the premix flame cannot stabilize at the desired position and subsequently propagates downstream, eventually causing the flame to blow-off. Thus, it leads us to the necessity to develop new technology to effectively stabilize the flame in the combustion chamber together with the swirler or bluff body while further reducing NOx/CO emissions compared to current levels without the use of expensive exhaust gas treatment units [32]. One of the most recently studied types of burners that are known to be good for stabilizing flames in lean conditions is low-swirl burners (LSB) [33–35]. Its working principle is based on the nature of the propagation of a turbulent premixed flame, and its basic premise is to stabilize the turbulent premixed flame as a stationary "standing wave" not associated with any physical surfaces [36]. This is achieved by creating a divergent flow, which is formed when the swirling intensity is below the vortex breakdown point. Thus, the LSB concept is fundamentally different from the high swirl concept, where vortex breaking is a vital prerequisite for creating a strong and reliable toroidal recirculation zone [36]. For practical applications, the LSB scheme has some major positive points, especially applicable for such fuels as LCV gas [34]. One of the abilities of such a design is to ensure that the flame cannot flashback into the burner when the velocity at the exit is higher than the turbulent flame speed [36]. Blow-off is also mitigated because the flame retreats to a lower-velocity region in the divergent flow when any sudden decrease in stoichiometry occurs. Additionally, the consequence of changes in mixture inhomogeneity or slight flow transients is a slight shift in the flame position [37]. Therefore, the likelihood of a blow-off is reduced substantially. The LSB flow field provides a self-adjusting mechanism for the flame to withstand transients and changes in mixture and flow conditions [38].

Reviewed literature shows that experimental data for plasma-assisted combustion of low calorific value gas are not common and there still exists a lack of knowledge. For this reason, this complex study focus on a combined PAC and LSB technology for low calorific gas combustion and experimental investigations were performed to determine the influence of the driving frequency of the plasma discharge and the excess air ratio on the swirling premixed methane-CO_2 flames. The

scientific novelty of the work consists of plasma application to enhance LCV gas combustion and research on the influence of the plasma frequency variation from 60 kHz to 120 kHz coupled with the influence of the air excess ratio parameter (Φ) to the leaner combustion regime on combustion properties of LCV gases, to find most relevant and profitable characteristics of plasma to achieve most stable combustion with least possible amount of undesirable gases emission.

2. Materials and methods

The experimental rig employed in this study comprises the combustion chamber and burner, along with measurement methods involving OH*, C_2*, and CH* chemiluminescence capturing ICCD camera, digital oscilloscope, and exhaust gas analysis system. Additionally, a pulse DC-type plasma generator is integrated into the setup.

2.1. Experimental rig and burner

The experimental rig consisted of a plasma-assisted low swirl burner, a high voltage pulse generator, mass flow controllers, the chemiluminescence capturing and flow gas analysis systems which are schematically shown in Fig. 1.

The plasma-assisted low-swirl burner (see Fig. 2) consists of a cone-shaped inner electrode with a diameter of 20 mm, which is connected to a high-voltage line. As a ground electrode serves a cylindrical body with an external diameter of Ø=28, the length of the body is 44 mm, and the main internal channel is Ø=22 mm. Both electrodes are made from stainless steel type 321.

In order to achieve highest possible mixing rates of gases, a system with a pre-mixing chamber was used. After mixing, gases were supplied to two radial-settled inlet nozzles with internal diameter of 6 mm. That

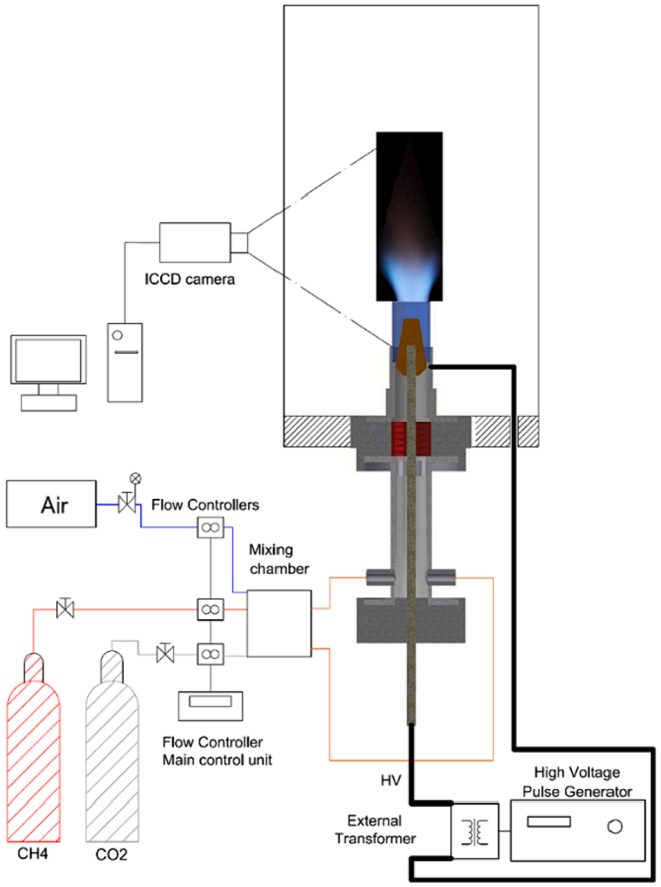

Fig. 1. Scheme of the experimental setup.

was made to allow the field of speeds to stabilize itself for ensuring relatively equal velocity of gas in the gap. After getting into the main burners body cavity, the gas mixture reaches the swirler, which has 10 vanes with a swirling number 0.637 for the swirler with flow exit of angle 40 degrees. Swirling flow moves all through the internal cavity of the burner until reaches the minimal gap cross-section. The arc is initially formed at the narrowest gap between the electrodes, and then elongated along the electrodes by the force of gas flow. The length of the gliding arc increases until its extinction unless the arc short-cuts a long current path with a shorter one. Though, the whole cross-section of the gas exhausting channel being covered with one or multiple layers of plasma arcs. By this method the rotating gliding arc plasma is generated. The experimental setup was installed on the table, covered with plexiglass wall-shields to ensure safety through the combustion process and decrease the possibility of leakage of the combustible gas or flue gases to the laboratory, instead of suction ventilation port. The plasma-assisted burner was shielded with the quartz glass tube with a diameter of 130 mm and height of 730 mm, which ensured a required light transmittance (>90 %) for the flame imaging by the ICCD camera.

Commercially available pure grade gases (methane and carbon dioxide) were used for preparation of synthetic biogas and compressed air was used as an oxidizer. Flow rates of gases were controlled using Brooks Instruments MFC controlling unit (Brooks 0254) and 3 mass flow controllers (Brooks SLA 5800) and directed to the mixing chamber. The overall flow was set to maintain constant burner thermal power changing the fuel equivalence ratio (Φ) and mixture composition. Main combustion parameters are presented in Table 1. The gas compositions for experiments were chosen considering the lowest and highest CH_4 amount in the biogas. The mixture with 25 vol% of CH_4 in CO_2 was chosen with the lowest calorific value, which is near the flame blow-off limit under normal conditions. The second mixture consisted of 60 vol% of CH_4 in CO_2 as common composition of biogas achieved in anaerobic digestion plants.

To create plasma discharge, a high voltage plasma generator G2000 (Redline Technologies) with a maximum voltage of 10 kV, frequency range 0–500 kHz and output power up to 500 W was used. The experiments were performed with a voltage of 4.66 kV and with four frequencies (60, 80, 100, and 120 kHz) to observe the influence of driving frequency on the combustion process. The range of frequencies were selected based on the obtained results in previous work[39]. It was found that the highest efficiency of the dry biogas reforming is achieved in the region of 60–120 kHz plasma discharge frequencies.

The theoretical thermal power of a burner calculated from the flow of the combustible gas is 1.23 kW. The power consumed by the plasma generator from the grid can be observed in Table 2.

Consumed power does not very much, and the consumption growth trend is linear. The amount of consumed electrical energy compared to the thermal power of the burner varies from 5.8 % to 11.46 %.

2.2. Burner swirler

The swirler is made by a 3D printing method from PLA + plastic, contains 10 veins, has a length of 22 mm, external Ø=26 mm and internal channel for the rode of the central electrode diameter of 8 mm Ri (for internal) and Ro (for outer) diameters, matched on Fig. 3, are used for calculating swirling number of the swirler. Ri = 10 mm and Ro = 22 mm accordingly. Angle φ represents the angle between the horizontal top plate of the swirler and the guiding vein plane and is equal to 40°.

$$S = \frac{2}{3} tg(\varphi) \bullet \frac{\left(1 - \frac{R_i}{R_o}^3\right)}{\left(1 - \frac{R_i}{R_o}^2\right)} \quad (1)$$

After calculating expression (1) for the angle of 40° swirl number S is equal to 0.637.

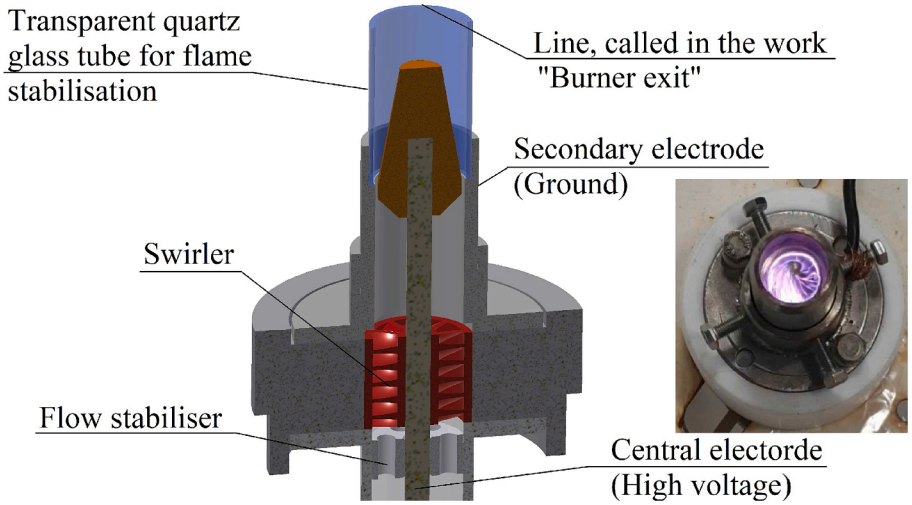

Fig. 2. Scheme of the low-swirl plasma assisted burner.

Table 1
The main parameters and gas flows used for combustion.

Gas composition	Excess air ratio, Φ	CH_4 l/min	CO_2 l/min	Air l/min
CH_4 −25 %; CO_2 – 75 % ($BG_{25/75}$)	0.83	2.22	6.6	25.14
	0.76	2.22	6.6	27.24
	0.71	2.22	6.6	29.33
CH_4 −60 %; CO_2 – 40 % ($BG_{60/40}$)	0.83	2.22	1.47	25.14
	0.76	2.22	1.47	27.24
	0.71	2.22	1.47	29.33

Table 2
Energy part for the plasma discharge formation.

Gas composition	Fuel equivalence ratio, Φ	60 kHz	80 kHz	100 kHz	120 kHz
CH_4 −25 %; CO_2 – 75 % ($BG_{25/75}$)	0.83	71 W	102 W	123 W	145 W
	0.76	73 W	96 W	117 W	144 W
	0.71	69 W	99 W	122 W	142 W
CH_4 −60 %; CO_2 – 40 % ($BG_{60/40}$)	0.83	73 W	101 W	124 W	140 W
	0.76	75 W	97 W	123 W	140 W
	0.71	70 W	94 W	122 W	135 W

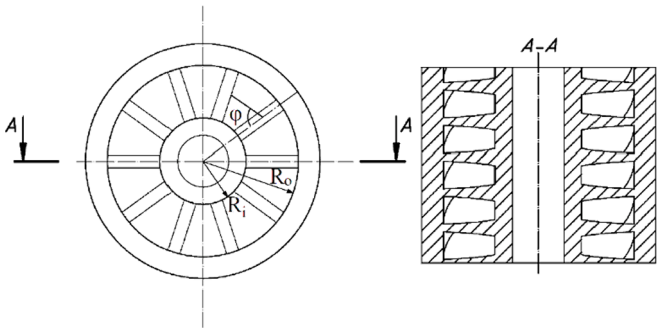

Fig. 3. Schematic view of the used swirler. Top view with shown dimensions that were used for calculation is presented on the left picture and cross-section view is presented on the right.).

2.3. Chemiluminescence and electrical characteristics measuring methods

The flame chemiluminescence of different mixtures was observed using a 1024 × 1024 pixels intensified charge-coupled device (ICCD) camera Andor iStar DH734 sensitive to 200–800 nm wavelength light. The camera consists of a photocathode with a diameter of 18 mm and a pixel size of 13 μm. Equivalent background illumination below 0.2 e-/pix/sec. The camera was directed to the burner and focused on the flame in such a way that the flame and burner nozzle fits the image frame entirely. The spatial distribution of excited OH* (310 ± 10 nm), CH* (387 ± 10 nm), and C_2* (514 ± 10 nm) from the flames were captured through the hard-coated bandpass filters mounted on the camera objective. The ANDOR SOLIS software was used to control the camera and store the acquired radiation intensity data. To compensate a emission intensity loss through the chamber made from quartz glass (transparency of 80–90 %) and through filters, and to reduce the effect of flame instability for each mixture and combustion condition, a single flame image was obtained by averaging 30 acquisitions with an exposure time of 0.04 s. The collected raw data was processed using the Python 3.6 software [40] using two scripts for flame visualization at different conditions with constant intensity scale and for the distribution of relative emission intensities of chemiluminescent species along the burner y axis. The visualization was made using Matplotlib function in Python, and the distribution of relative emission intensities was obtained using a Python script by averaging each horizontal line of pixel intensity values in the frame.

For acquiring current and voltage, a digital oscilloscope Rigol DS4014 was with a High Voltage probe Tektronix P6015A and a current measuring probe. The increment parameter was set at 5·10-8 s to ensure that a couple of peaks would be collected through each acquisition process to avoid an error that would be connected to the fluctuation of the parameters.

2.4. Flue gas analysis

A flue gas sampling probe was installed inside the chamber at a distance of 60 cm from the burner surface for sampling. The probe was installed in the metal cap that covered quartz glass on the central axis. The Testo 350XL analyser was connected to the sampling probe to measure emissions of NOx and CO in flue gas. Every sampling test took 120 s for parameter stabilization.

3. Results and discussion

3.1. Plasma discharge characteristics

Due to the non-linear increase in a radical generation rate with a linear increase of the driving frequency, it was decided to determine plasma pulse characteristics using the high voltage and current probes. Fig. 4 and Fig. 5 show the volumetric energy, current and voltage of discharge versus time respectively for mixtures of $BG_{25/75}$ and $BG_{60/40}$. The volumetric density of the plasma is important characteristic showing the amount of energy being transferred to the gas from the source per one period. From Fig. 4 and Fig. 5, it was found that the highest volumetric density was determined for the 80 kHz regime, reaching 3.305 J/m^3 for $BG_{25/75}$ and 3.167 J/m^3 for $BG_{60/40}$, respectively. In overall, the 80 kHz peak of the $BG_{25/75}$ showed higher energy density compared to peaks in 60 kHz, 100 kHz and 120 kHz regimes. The excess of volumetric energy density for the 80 kHz regime over the other used regimes with different driving frequencies (60, 100 and 120 kHz) was 26 %, 45 % and 53 %, respectively. For mixture of $BG_{60/40}$, the trend was similar, and the volumetric energy density at 80 kHz discharge differed 16 %, 51 % and 69 %, respectively at 60 kHz, 100 kHz, and 120 kHz regimes. Regarding discharge parameters, it could be noted that both current and voltage peaks for 80 kHz (for both mixtures) reach the highest values compared to the other driving frequency discharge characteristics. That could also probably happen due to so-called "short-cutting event» which were mentioned in the work [41]. When it occurs, the discharge current increase from mA to Amperes which could also influence thermal or kinetic mechanism. It should be noted that while discharge periods for both $BG_{25/75}$ and for $BG_{60/40}$ were trending to decrease and the difference between the period for each mixture was not exceeding 0.05 μs, for 80 kHz, the period for $BG_{25/75}$ was 0.4 μs shorter, comparing with the corresponding period for the 80 kHz driving frequency for $BG_{60/40}$. In addition to determine the pathway of plasma enhancement, the temperature of the cone rode under plasma influence was measured and specific energy input (SEI) for both $BG_{25/75}$ and $BG_{60/40}$ mixtures was calculated (see Fig. 6.).

The temperature of the inner cone was measured while plasma was rotating under the influence of the air (carrier gas) and CO_2 maintaining the overall flow used in the research. According to obtained results (Fig. 6), the temperature of the inner rod increased linearly with the

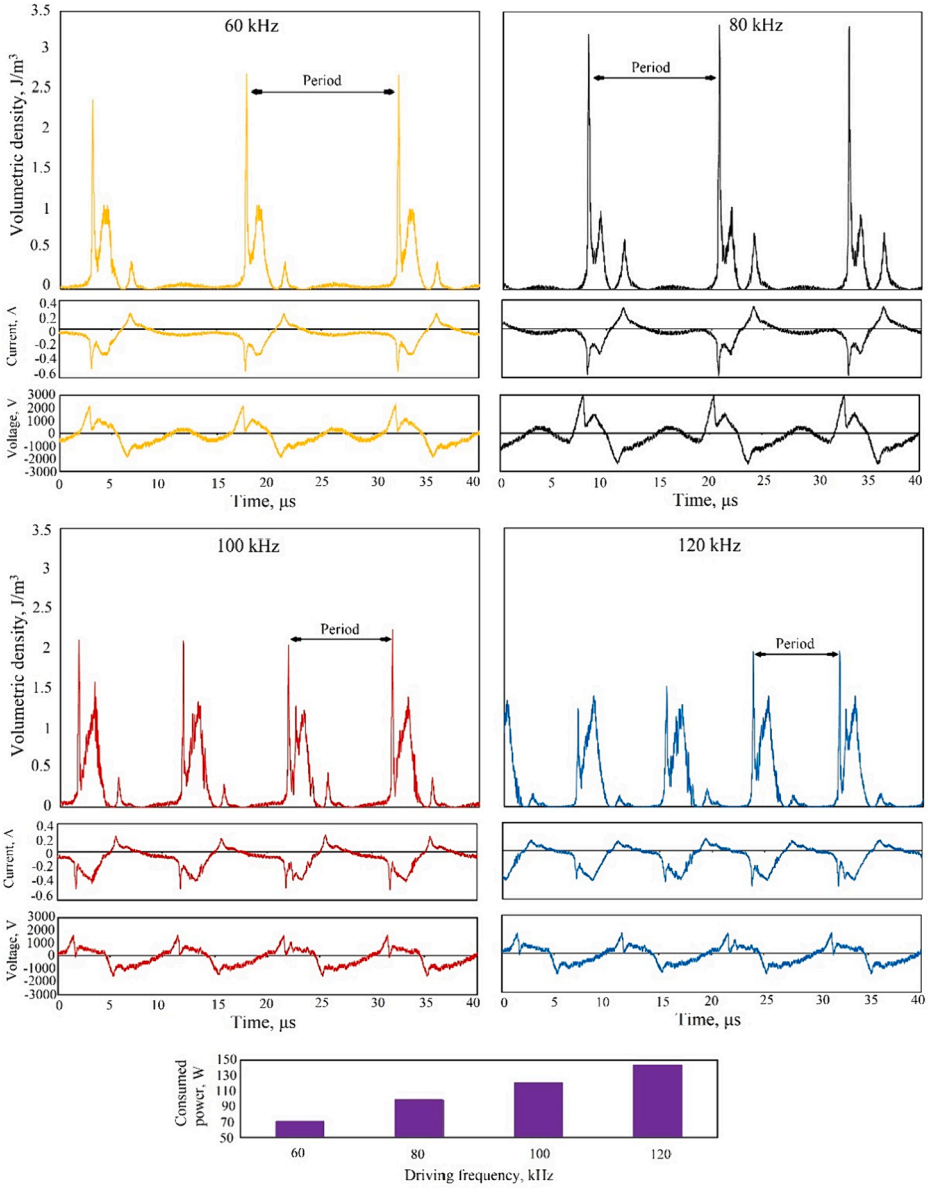

Fig. 4. Energy density, current and voltage of the discharge in the relation to the pulse duration in μs, for the $BG_{25/75}$.

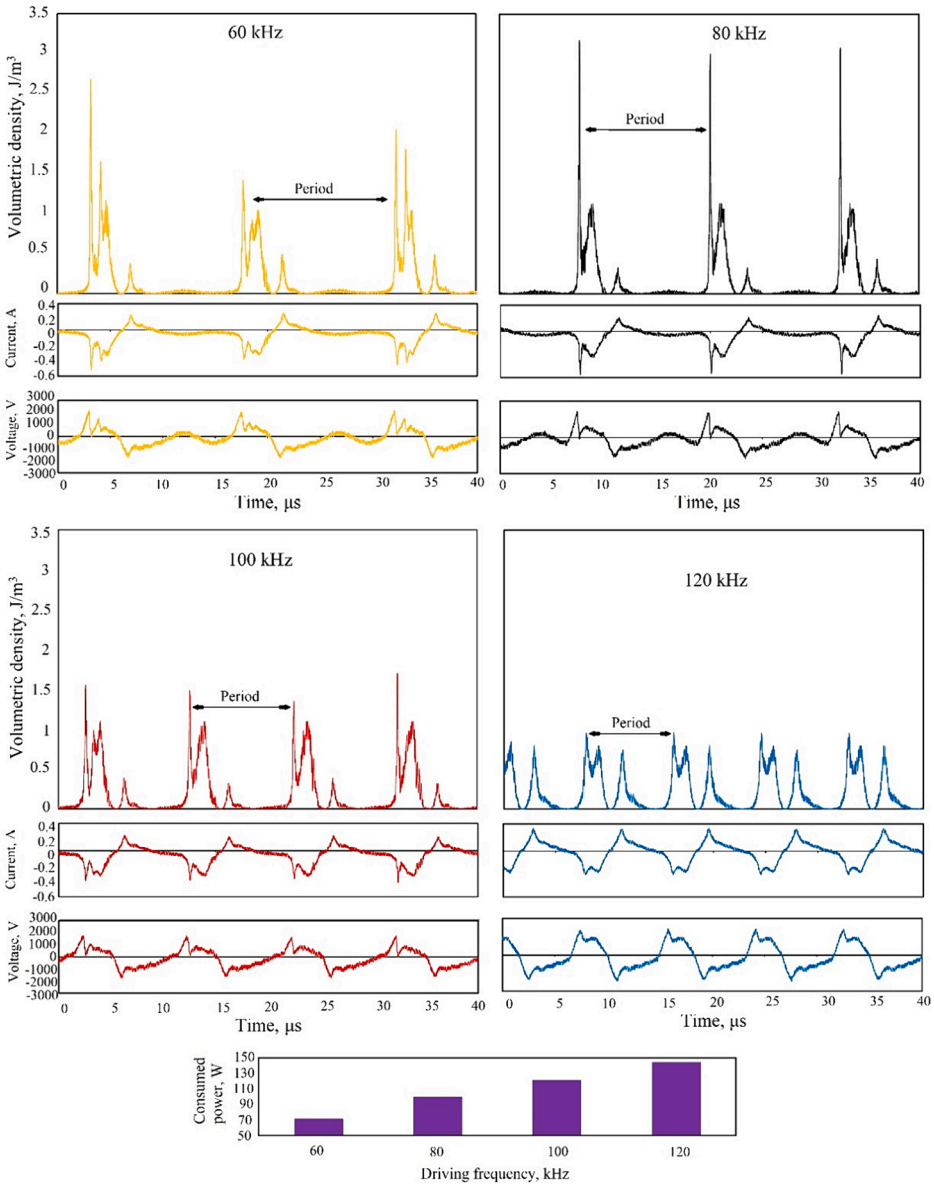

Fig. 5. Energy density, current and voltage of the discharge in the relation to the pulse duration in μs, for the $BG_{60/40}$.

driving frequency. Though, a higher CO_2 content in the mixture leads to cooling effect and decreased influence by plasma in terms of reduced SEI as overall flow increases. Through the Townsend mechanism, the reduction of SEI reduces a collision rate for inelastic collisions and vice versa. For example, for reactions with low activation energy, vibrational excitation is one of the most possible mechanisms. The chemical reaction $CO_2 \rightarrow CO + ½\ O_2$ is obtained at the enthalpy of CO_2 dissociation, ΔH, of 2.9 eV. The energy transfer in the plasma comprises direct electron dissociation or dissociation through the so-called vibrational "ladder climbing" [42]. The direct electron impact dissociation in the plasma occurs at a threshold energy of about 7 eV with a further contribution at about 10.5 eV, which is noticeably higher than the dissociation energy to break one C–O bond in CO_2 of 5.5 eV [43]. To enable CO_2 conversion into CO at reduced energies, a plasma-chemical reaction pathway involving many vibrationally excited states, CO_2*, with small energy gaps and collisions among them can be exploited allowing dissociation at 5.5 eV resulting in the vibrational ladder climbing. Moreover, conditions that favour the further reaction of the generated side product, atomic oxygen, with CO_2 yield another CO molecule converted at 0.3 eV, resulting in the overall specific energy requirement (threshold energy) of about 2.9 eV [44]. At the same time, the energy required for plasma-assisted methane conversion in gliding arc conditions is much smaller, around 1.6 eV [45]. Because of that, while generating a relatively high number of charged particles at low frequencies, the energy of the particle was not high enough to convert higher rates of CO_2.

3.2. *Flame characteristics*

The experiments were carried out with two mixtures containing different CH_4 level in CO_2: 60 % of CH_4 ($BG_{60/40}$) as biogas and 25 % of CH_4 in CO_2 ($BG_{25/75}$) as low calorific value gas. The obtained images of flames using a digital camera are presented in Fig. 7. In the case of the $BG_{25/75}$ mixture, the presence of CO_2 negatively affected flame stabilization due to reduced flame temperature [46], resulting in hydrodynamic and diffusive-thermal instability and changes in flame structure.

Moreover, this mixture was hardly combustible under normal conditions without plasma assistance compared to the case of $BG_{60/40}$. The flame length decreased linearly changing ϕ from 0.83 to 0.71 and the flame fluttering occurred at the leanest fuel condition resulting in blow-

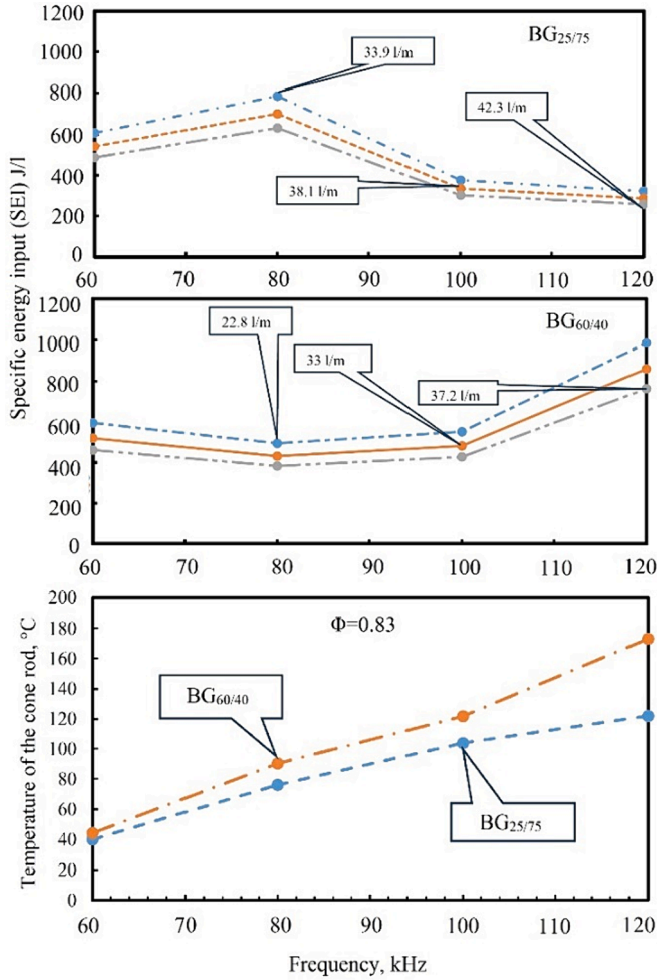

Fig. 6. The specific energy input and temperature of the inner cone-shaped electrode versus the driving plasma frequency.

off. Meanwhile the biogas flame ($BG_{60/40}$) was stable and the flame width was only decreasing approaching to leaner combustion conditions. In the case of plasma-assisted combustion, the flame stability of $BG_{25/75}$ was improved and the effect was more intense with increasing discharge frequency (Fig. 7). This effect was observed in the case of biogas flames as well (Fig. 7). In addition, in both cases the flame length increase and flame color changes were observed during plasma-assisted combustion with increasing discharge frequency. According to Zhang et al. [47], the visual flame extension increasing the plasma power is related to the increased flame temperature and intensified OH* formation in flames. It also could be proven by images of biogas flames as increasing discharge frequency leads to more intense orange color in the flame top caused by luminous emission from heated burner exit made of quartz. In this particular case, the intensified soot formation is rejected as obtained CO emissions decrease with increasing discharge frequency. Besides, many studies related to plasma-assisted combustion prove that plasma leads to suppression of soot formation [48–50].

For better understanding on plasma influence on flame characteristics, the spatial emission of OH*, C_2* and CH* from flame chemiluminescence were observed by the ICCD camera and the obtained data was converted to flame images with equal intensity scale for OH*, C_2* and CH* (see Fig. 8 and Fig. 9). In the case of ($BG_{25/75}$), the spatial emission of obtained OH*, C_2* and CH* shows that high dilution of CO_2 which in turn decreases the flame temperature and speed leads to decreased intensities compared to $BG_{60/40}$ flame (Fig. 8). Although, the chemiluminescence of C_2* well corresponds to the flame structure and its changes from wide to narrow one due to increasing CO_2 level in the mixture. Besides, during experiments it was noted that the proposed burner configuration has a major impact on the flame stability and flammability as well. Even though the flame of $BG_{25/75}$ was near the blow-off limit at tested ϕ values (see Fig. 7), the burner construction ensured combustion of high CO_2 dilution (75 vol%) mixtures. For example, such composition gases were only combusted under oxygen or syngas-enriched conditions in the different configuration LSB burner [51] and flat flame one [52].

During the plasma-assisted combustion, the shape of $BG_{25/75}$ flame becomes wider and the flame structure closely resembles to a leaner flame of $BG_{60/40}$ without plasma assistance (Fig. 9 and Fig. 8), especially at higher frequencies indicating the enhancement in the flame stability. Analyzing spatial emission of OH*, it is observed that emission intensity is higher in the plasma discharge point than in the flames and with increasing frequency, the spatial emission intensifies. That also correlates with determined core temperature increase caused by the plasma discharge (Fig. 9) and could be related to thermal effect of plasma. Effect of the positive influence of the temperature rise on the rates of OH* radical generation was also observed by Feng et al. [53]. Such conditions can support effective excitation to vibrational states, which can lead to the so-called ladder-climbing effect [54] described in the section above. Although, optical emission spectroscopy diagnostics of the CH_4/CO_2 mixtures performed in the previous research [39] revealed that highly reactive species and radicals from fuel such as OH, CO, H_2, etc. and from oxidizer such as singlet oxygen O_2 ($a1\Delta g$) are produced due to plasma discharge. Moreover, it was determined that lower concentration of CH_4 in CO_2 leads to more intense reforming to H_2/CO by plasma discharge and vice versa [55,56]. Also, the presence of singlet oxygen from the oxidizer group in the plasma discharge could lead to an increment of the flame-covered zone [57] and as well as more intense fuel oxidation leading to a higher flame temperature with the result of increased OH* intensities [58–60]. The proposed mechanism also relates to increased spatial emissions of C_2* and CH* from flames with the increasing plasma discharge frequency. Contrary to OH* emissions, C_2* images clearly indicate the plasma discharge area and the flame area. Based on that it is observed that with increasing frequency from 60 to 120 kHz, the flame shifts closer to the cone (Fig. 9). Especially for $BG_{60/40}$, the highest emission intensity is observed at the cone at 120 kHz with changed flame shape indicating high influence by the plasma assistance. Though spatial emission of CH* overlaps with plasma and flame caused chemiluminescence, but plasma intensified chemiluminescence of CH* at the plasma discharge point is highest only for $BG_{25/75}$ flames. According to the results, it happens due to a higher overall flow, which causes a formation of the gliding arc at the cone top resulting in the lower specific energy density compared to other cases (Fig. 6). Despite that, the highest emissions of CH* were observed above the burner exit and also increased with plasma discharge frequency compared to the case without plasma assistance (Fig. 8). According to [61], the increased intensity could be attributed to higher flame temperature. In this case, that explains the flame movement closer to the cone with increasing plasma frequency, but considering that the heating effect by plasma discharge is linear (Fig. 6), it could be assumed that at higher frequencies dominates the kinetic effect of plasma discharges leading to reforming of the mixtures.

Also the raw data obtained by the ICCD camera were processed using the Python software by averaging rows in the matrix of intensities and the distribution of averaged emission intensities of three studied radicals (OH*, C_2*, CH*) per height were determined and attributed to the position from the burner body including an indication of the cone rod and burner exit (see Fig. 10 and Fig. 11). The estimated profiles demonstrate the emission intensity distribution without plasma assistance and their changes in response to altered driving frequency (from 60 kHz to 120 kHz). The data of plasma-assisted combustion reveal two distinct peaks: one located beyond the “burner exit” line and another above it. This can be explained by the lower peak being generated by the plasma discharge observed via the ICCD camera due to used burner nozzle made of the

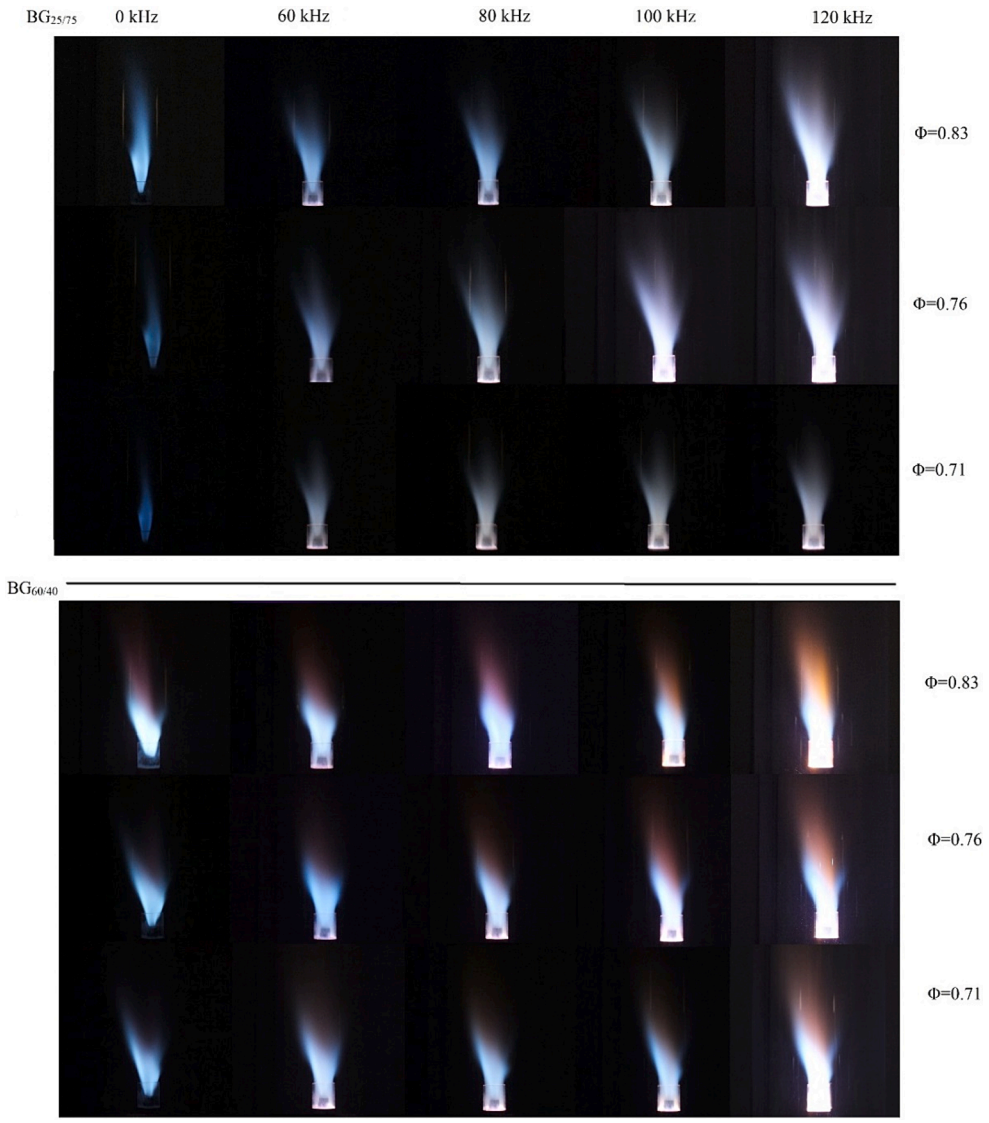

Fig. 7. Images of BG25/75 and BG60/40 flames with and without plasma assistance versus ϕ.

quartz glass. The upper peak represents the "flame kernel" position, where the intense fuel oxidation leads to the highest radical production as it was determined in the previous work [62]. For the combustion of $BG_{25/75}$, the spatial distribution of OH* extends further towards the base of the flame, but due to high CO_2 dilution resulting in reduced flame temperature, the emission intensities above the burner exit keep considerably low.

With increasing discharge frequency from 60 to 120 kHz, increase of OH*, C_2* and CH* emissions were obtained. Due to the averaged emission intensities, the estimated effect of plasma was considerably low, from 0.13 to 0.48 %, from 0.29 to 0.56 % and from 0.66 to 1.05 % respectively for OH*, C_2* and CH*. Approaching to leaner combustion condition, the plasma discharge influence on the radical emission intensities was decreasing linearly by about 10 %. Besides, analysing the data, was determined that increasing frequency does not correspond to intensities in the plasma discharge area and in the flame middle (Fig. 10).

The averaged emission intensity is the highest in the plasma discharge area (below the cone) at 120 kHz, but the averaged emission intensity at this frequency in the flame area is similar or close to one at 100 kHz. Analysing the plasma-assisted combustion of $BG_{60/40}$, it is determined that emission intensities of C_2* and CH* increase non-linearly with increasing driving frequency from 60 to 120 kHz, reaching a local maximum at the 80 kHz plasma regime, decreasing at 100 kHz, and resuming an increasing trend at 120 kHz (Fig. 11). The exceptional behaviour of some frequencies among others is considered by the difference in SEI (specific energy input) levels. Potentially, the decrease of the SEI parameter with the increase of the flow rate could make the effect of the plasma on the radical generation smaller, which was assumed in [63]. That would explain, for the 60 kHz regime the averaged emission intensity values of OH* and C_2* decrease by 0.38 % and by 0.03 % at $\Phi = 0.83$, but increase at higher frequencies. Increasing the discharge frequency from 80 to 120 kHz, the plasma influence becomes positive as the SEI increase (Fig. 6) and OH* radical increases from 0.33 % to 0.61 %, C_2* increases from 0.21 % to 0.34 %, and CH* increases from 0.58 % to 0.6 %, respectively. Though the determined increase is considerably low, the flame position based on maximum values is determined between the cone and the burner exit indicating improved flame stability. Besides this effect was determined increasing frequency from 80 to 120 kHz. Considering higher SEI at higher frequencies (Fig. 6), this trend could be caused increased CO selectivity due to plasma reforming leading to more intense formation of CH* and increased flame temperature which affects the flame position [64,65]. According to He et al. [66], the generated C_2 and OH radicals influence the formation rates of CH* through the reaction ($C_2 + OH \rightarrow CH^* + CO$) [67].

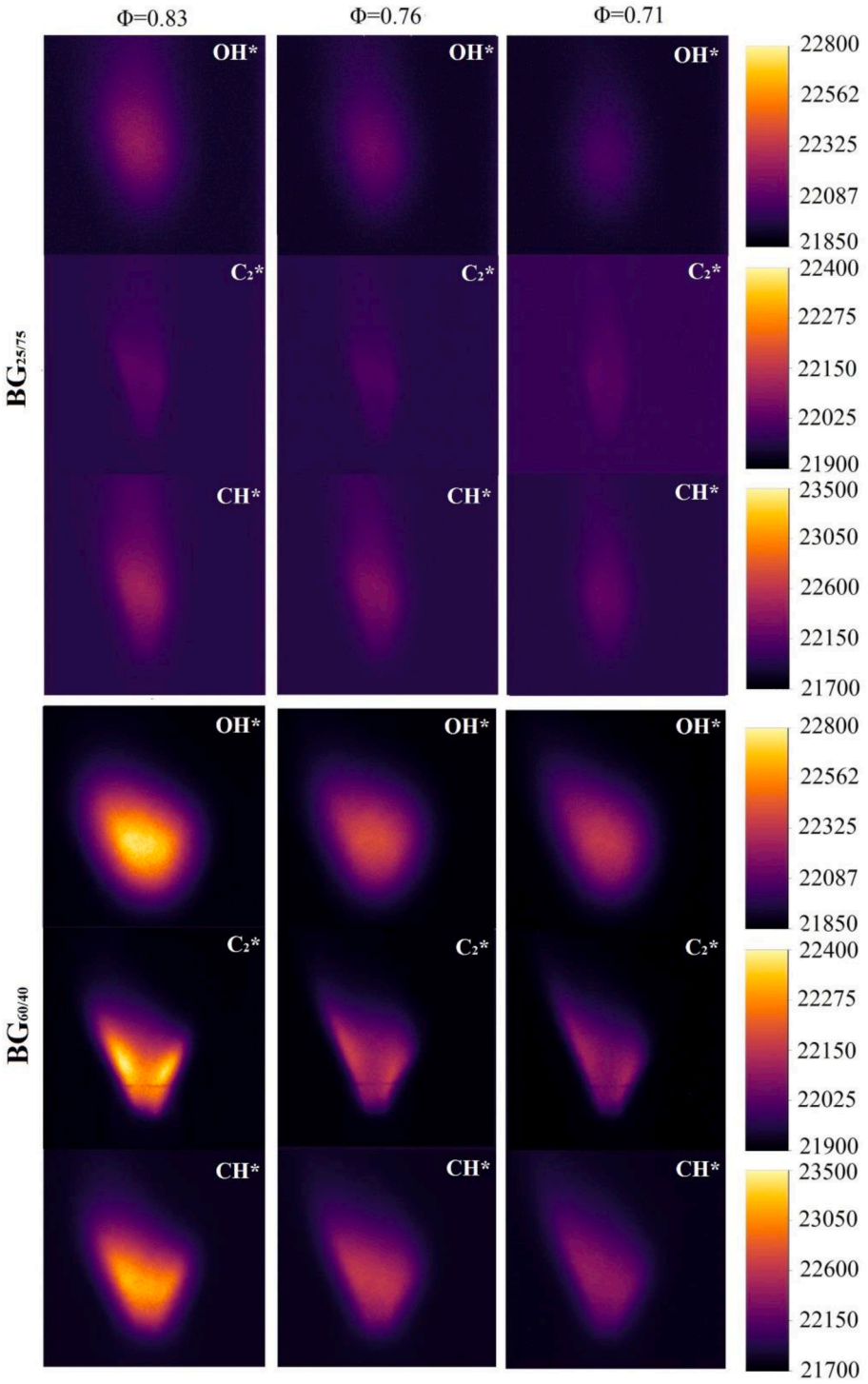

Fig. 8. Flame images of different composition mixtures without plasma assistance versus fuel equivalence ratio ϕ.

According to profiles of average emission intensities of registered radicals (Figs. 10 and 11), the flame-lift heights were estimated from C_2* and CH* emissions. The estimation from OH* emissions was rejected as these emissions were most affected by electron impact from plasma discharge and was complicated to precisely evaluate the flame kernel shift with changing combustion conditions in terms of plasma discharge frequency and fuel equivalence ratio.

3.3. Plasma influence on flame lift-off parameter

The highest values of averaged intensities of the C_2* and CH* were attributed to the main reaction zone in the flame and the distance from this position to the burner exit was considered as the flame lift-off height [62]. The flame lift-off heights for different mixtures at Φ values ranging from 0.83 to 0.71 and plasma discharge frequency ranging from 0 to 120 kHz are presented in Fig. 12. In the case of $BG_{25/75}$ (Fig. 12), the flame lift-off height by C_2* and CH* was negatively affected by plasma discharge of 60 kHz at $\Phi = 0.83$ as the flame position increased by 0.44 % and by 1.5 % respectively compared to the case of 0 kHz. This could be caused by electron wind increasing the vortex of the flame.

Increasing the plasma frequency from 80 to 120 kHz, flame lift-off was reduced from 2.43 to 16.34 % and from 1.71 to 1.5 % by

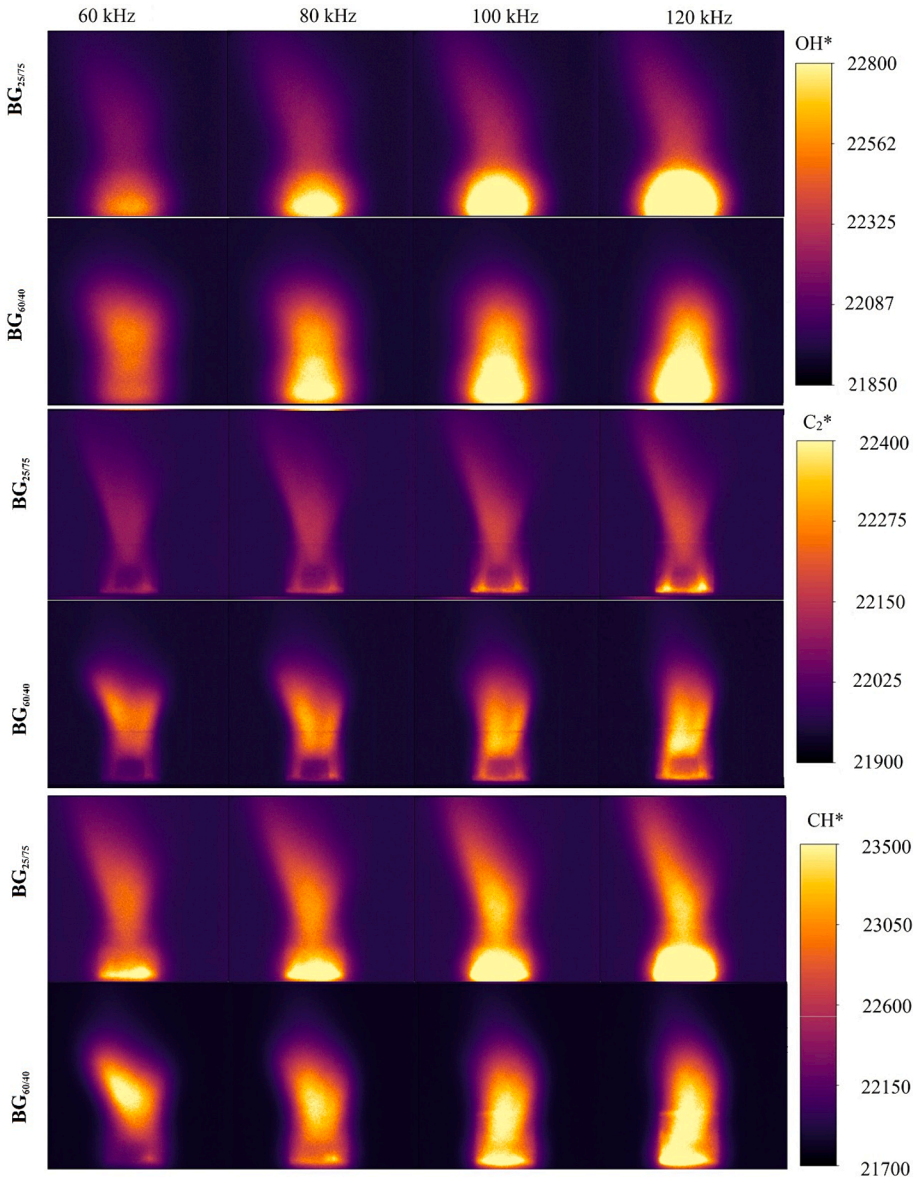

Fig. 9. Flame images of different composition mixtures under influence of 60–120 kHz plasma assistance at $\phi = 0.83$.

averaged maximum values of C_2* and CH* compared with non-assisted combustion. When moving towards leaner combustion conditions ($\Phi = 0.76$), the flame position is brought closer to the burner exit by 1.1 % compared to the $\Phi = 0.83$ without plasma assistance. The overall behaviour of the lift-off position remains the same but shows bigger influence of the plasma assistance on the combustion process: After applying the plasma, the flame lift-off decreased by 2.23 % and by 1.08 % based on C_2* and CH* values compared to regimes without plasma and the 60 kHz regime. Changing the plasma frequency from 80 to 120 kHz, the flame lift-off height decrease varied depending on the frequency from 13.17 % to 12.5 % by C_2* and from 1 to 15.5 % by CH* while significant improve was achieved at 100 kHz discharge by 16 % and by 18.5 % respectively compared to the case without plasma (Fig. 12). For the leanest conditions ($\Phi = 0.71$), the flame position shifted downward by 12.80 % and by 13.90 %, compared with $\Phi = 0.76$ and $\Phi = 0.83$, respectively. After applying plasma, the flame lift-off height by C_2* increased by 1.54 % though by CH*, the flame lift-off height was reduced by 7.31 % compared to regimes without plasma. Changing the plasma frequency from 80 to 120 kHz, the flame lift-off height was only reduced by 3.33 % based on C_2* while CH* pattern indicated significant improvement from 9.7 to 24.5 % compared with the regime of 0 kHz (Fig. 12). Notably, for gas mixtures with higher calorific value ($BG_{60/40}$), the influence of plasma assistance on stability was more significant increasing the discharge frequency as the SEI was increasing for this mixture compared to $BG_{25/75}$ (Fig. 6). Besides during combustion of $BG_{60/40}$, the flame position without the plasma assistance was located approximately 2.6–2.8 cm from the burner exit. Contrary to $BG_{25/75}$, the flame position shifted up with increasing fuel equivalence ratio (Fig. 12). Evaluating the flame lift-off height by C_2*, the plasma influence for $BG_{60/40}$ was weaker at frequencies of 60 and 80 kHz. It reflects determined SEI values for both mixtures (Fig. 6). Changing plasma frequency from 80 to 120 kHz, the flame lift-off height decreased from 3.57 % to 51.28 % compared with the 0 kHz regime resulting in significantly improved flame stability at 120 kHz. At the same time, at 60 kHz regime the flame position was influenced negatively and shifted up by 7.7 % compared to the case of 0 kHz regime (Fig. 12). Approaching to leaner fuel condition ($\Phi = 0.76$), the flame position shifted up by 29.9 % compared to the case of $\Phi = 0.83$. As in the previous case, the flame position was lifted at 60 kHz regime compared to flame lift-off heights without the plasma assistance. Despite that,

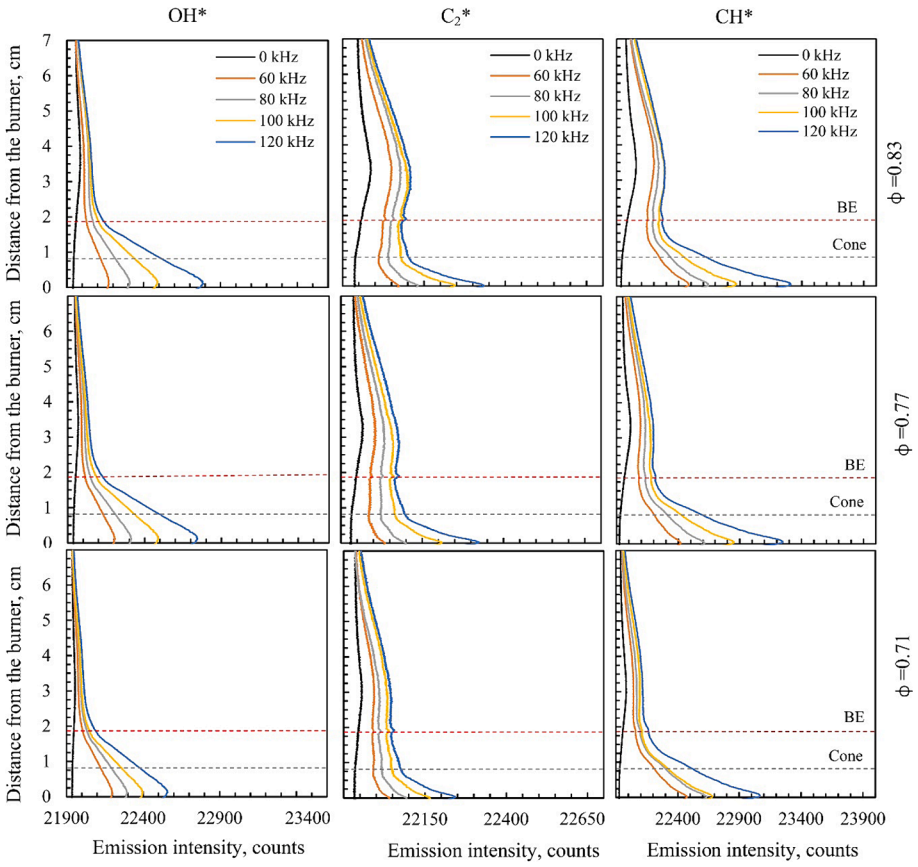

Fig. 10. Distribution of emission intensity of OH*, CH* and C_2* for $BG_{25/75}$.versus ϕ and driving frequency.

changing the plasma frequency from 80 to 120 kHz, the flame lift-off height decreased from 3.6 to 51.28 % compared to the position at 0 kHz. At the leanest regime (Φ = 0.71), the flame position shifted up as well by 4.2 % at 60 kHz regime compared to the regime without plasma. As in the previous case, the highest improvement by the plasma discharge was achieved at 120 kHz by 46.3 %. At the same time, CH* exhibited similar behaviour with linear pattern resulting to the most proposing impact on the flame lift off-height reduction from 18.4 to 25.5 % at 120 kHz regime approaching to leaner fuel condition from Φ = 0.83 to 0.71. Besides plasma assisted combustion of $BG_{60/40}$ indicated higher impact on the flame lift-off height reduction (by 8.18 % at 60–80 kHz; by 13.08 % at 100 kHz) at Φ = 0.71 compared to the case of $BG_{25/75}$ as it corresponds to the pattern of the SEI.

3.4. Pollutant emissions from plasma-assisted combustion

The gas analysis was done to determine the influence of plasma and fuel equivalence parameters on the emissions of nitrogen oxides and carbon monoxide. The obtained results indicate that the plasma impact negatively affects the NOx generation, forcing the emission intensity to rise (Fig. 13). Without plasma assistance, NO, NO_2 and NOx emissions were 3 ppm, 2.2 ppm and 6 ppm, respectively. Low emissions were obtained due to high content of CO_2 resulting in decreased rates of thermal NO formation. During the plasma-assisted combustion, for the same fuel equivalence ration, NO, NO_2 and NO_x raised up to 90 ppm, 123 ppm and 230 ppm, respectively (Fig. 13). For Φ = 0.76 without plasma influence, those were 3 ppm, 3.9 ppm and 7 ppm for No, NO_2 and NO_x accordingly, and for Φ = 0.71 without plasma influence, emissions were 8 ppm, 24 ppm, and 33 ppm accordingly. As it was expected, the emission level slightly drops on higher plasma regimes at leaner conditions, while for combustion without plasma assistance, the trend was the opposite. For Φ = 0.76, NO_2 production on the 120 kHz regime was 95.5 ppm, while on the 60 kHz regime, it was 101 ppm, which makes a 5.4 % decrease in oxide emission. While decrement of the parameter was observed for each fuel equivalence ratio, only for Φ = 0.76 did it reach values on the highest tested plasma regime (120 kHz), which were lower than on the weakest (60 kHz) plasma regime (Fig. 13). For Φ = 0.83, the change of the NO_2 emission intensity was 14.5 % to the rising side, and for Φ = 0.76, it was 9.8 % to the rising side, comparing emissions on 60 kHz and 120 kHz accordingly. At the same time, NO trends to increase. Active decreasement of NO_2 and increasing levels of NO at the high driving frequency can be explained by more intense thermal effect caused by plasma discharge (Fig. 6).

The measured carbon monoxide emissions are presented in the Fig. 14 and indicates the combustion performance of investigated mixtures. It could be seen that due to too low ambient temperature in the case of plasma-assisted combustion of $BG_{25/75}$ mixture, CO emissions were extremely high, up to 8000 ppm. The general trend of emission levels reacting to the plasma regime could still be observed. Such high levels of carbon monoxide emissions could probably be explained by an insufficient temperature in the combustion chamber, which was not ensuring the auto-ignition of CO. At 0 kHz (regime without plasma assistance) CO emissions for the $BG_{25/75}$ mixture were 3580, 2286 and 2456 ppm for Φ = 0.83, 0.76 and 0.71 respectively. During combustion of $BG_{25/75}$, CO emissions at tested Φ values (0.83, 0.76, 0.71) were higher in the case when 80 kHz driving frequency was applied (6556, 5022 and 4066 ppm, showing the increase by 45.3, 54.4 and 39.6 % for Φ = 0.83, 0.76 and 0.71 respectively) and then dropped down by 19, 18.6 and 14.8 % respectively when the discharge frequency of 100 kHz was applied. At highest applied driving frequency CO emissions were 7750, 5200 and 4966 ppm for Φ = 0.83, 0.76 and 0.71 respectively, exceeding the values for 0 kHz regime by 116, 127 and 102 % respectively. At the same time, the situation for the gas mixture with a higher calorific value was diametrically opposite. Considering that determined

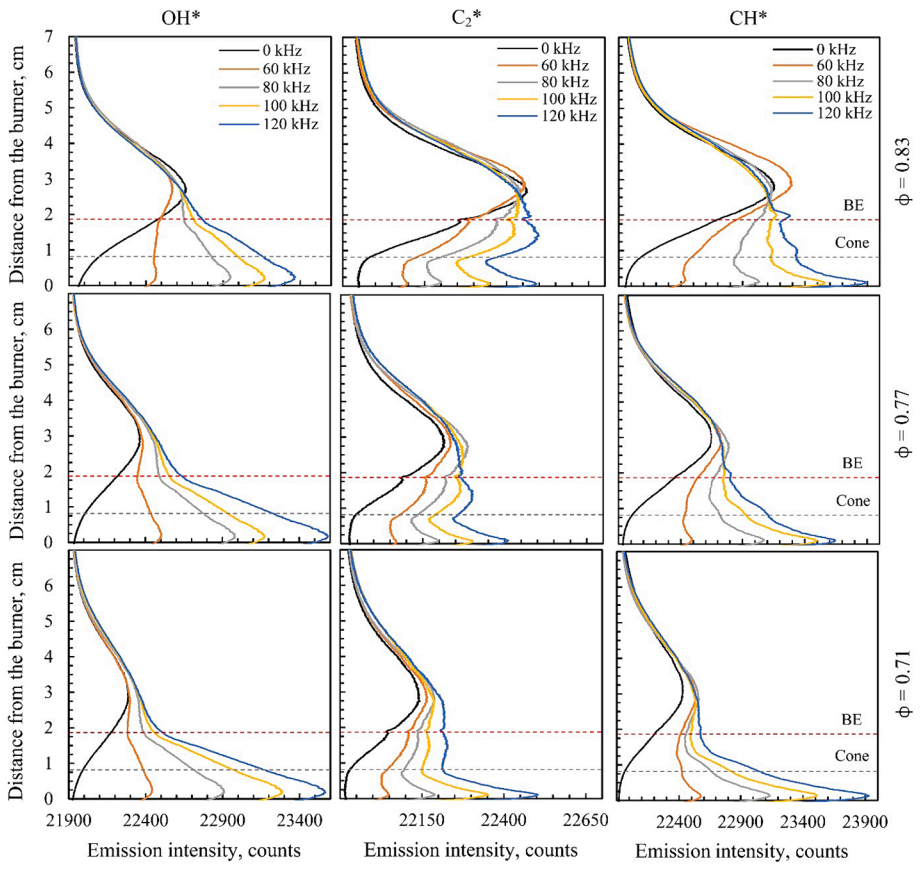

Fig. 11. Distribution of emission intensity of OH*, CH* and C_2* for $BG_{60/40}$.versus ϕ and driving frequency.

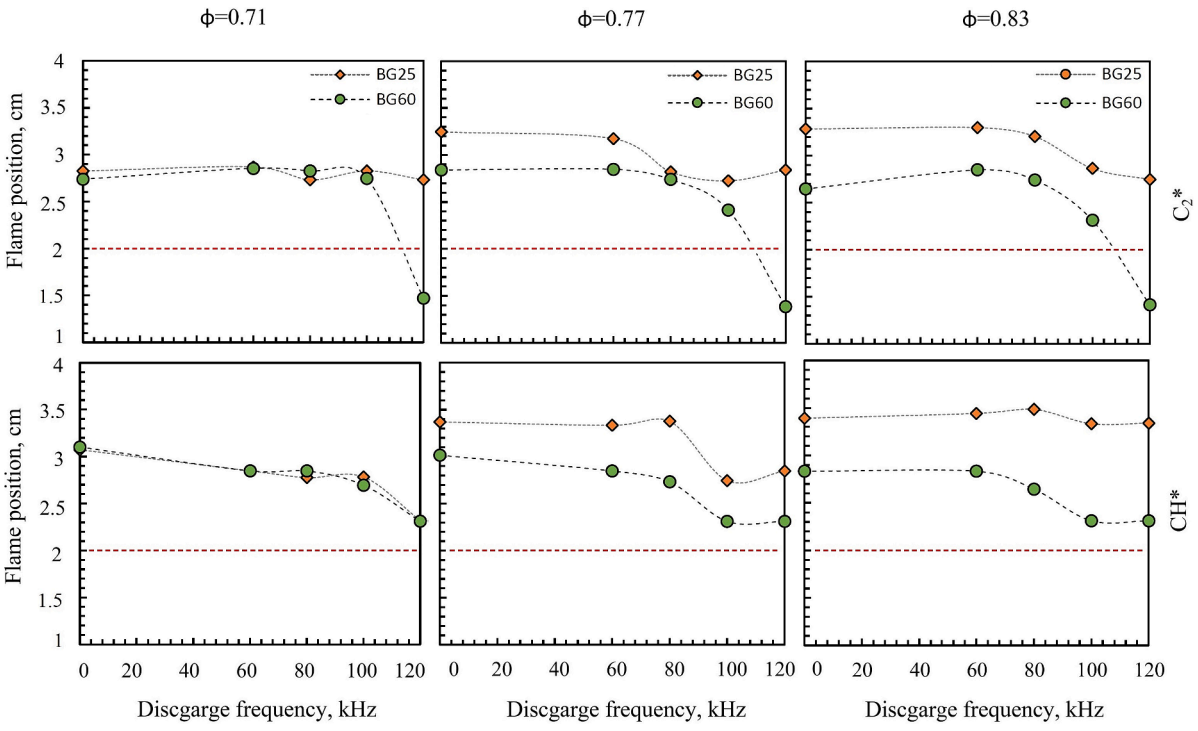

Fig. 12. Flame lift-off heights during combustion of $BG_{25/75}$ and $BG_{60/40}$ with and without plasma assistance versus Φ.

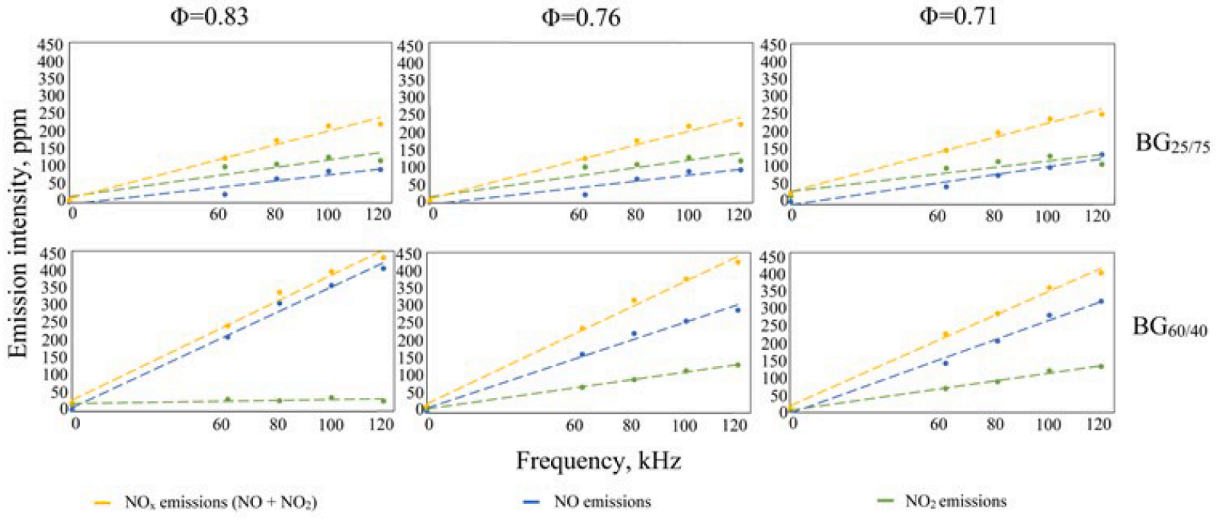

Fig. 13. Emissions of NO, NO_2 and NO_x under different plasma and air excess ratio parameters for $BG_{25/75}$ and $BG_{60/40}$.

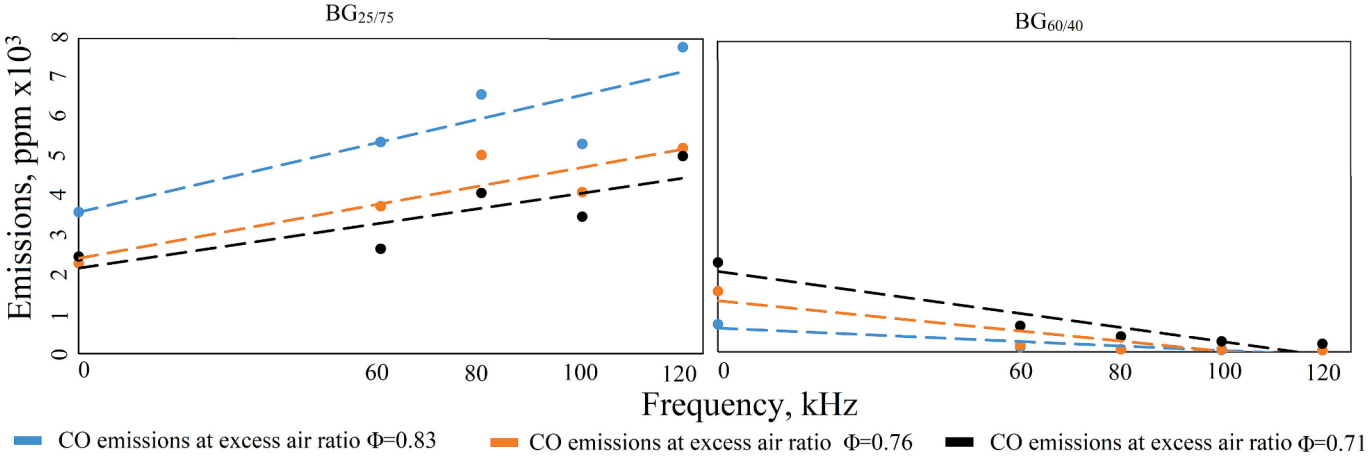

Fig. 14. Emissions of CO under different plasma and air excess ratio parameters for $BG_{25/75}$ and $BG_{60/40}$.

emissions of OH*, C_2* and CH* radicals (Fig. 11) were higher in the flame zone compared to the case without plasma assistance, the plasma effect could be attributed both to kinetic and thermal effect as it leads to higher conversion rates of CO_2 to CO in the discharge which improved combustion stability and also the electron impact causes the flow heating as the cone temperature increases (Fig. 6). In that way, changing the frequency from 60 to 120 kHz, emissions decrease from 700 to 45 ppm at $\Phi = 0.83$ was determined. It indicates 93.5 % decrease in emissions level while comparing 120 kHz regime and regime without plasma assistance and 82.8 % while comparing 60 kHz and conventional combustion regimes. At leaner combustion conditions, CO emissions were higher as the flame temperature decreased. CO reached the level of 1537 ppm at $\Phi = 0.76$ without the plasma assistance while under the 60 kHz assistance regime, CO was 167 ppm, and at the 120 kHz regime, the level of emissions was 46 ppm (Fig. 14). For the leanest fuel condition ($\Phi = 0.71$), CO emissions at normal combustion conditions reached 2267 ppm and were reduced by the plasma discharge till 665 ppm and 210 ppm for 60 kHz and 120 kHz regimes respectively. The plasma-assisted combustion of $BG_{60/40}$ led to improved combustion efficiency as CO emissions were reduced by 70.2 % for 60 kHz and 90.7 % for 120 kHz, respectively.

4. Conclusions

In this study, the impact of plasma assistance on swirled premixed CH_4/CO_2-air flames was investigated. The configuration of the burner contains swirler in the central part of the burner, through which the central high-voltage electrode is mounted. The burner is equipped with a closed cylindrical chamber made from quartz glass, which was designed to utilize low-calorific value gas (biogas $BG_{25/75}$ with methane concentration 25 %) as primary fuel and biogas $BG_{60/40}$ (with methane concentration 60 %) as reference point gas. The influence of plasma assistance on the combustion process of low calorific gas and biogas with concentration on flame stability and radical emissions was reported and discussed. The driving frequency varied from 60 kHz to 120 kHz with a step of 20 kHz. Based on the obtained results, the following conclusions can be provided:

Plasma frequency increase leads to OH*, C_2* and CH* emissions enhanced in the flame. For $BG_{25/75}$ while comparing 80 kHz and regime without assistance OH*, C_2 and CH* emission intensification was by 0.28 %; 0.41 % and 0.82 % respectively for $\Phi = 0.83$. For 120 kHz regime emission intensification was by 0.47, 0.55 and 1.04 % while energy consumption for the 120 kHz regime was 30.7 % higher. For leaner $\Phi = 0.76$ and $\Phi = 0.71$, intensification of the same radicals was 0.24 %, 0.30 %, 0.54 % and 0.23 %, 0.25 %, and 0.39 %, respectively for 80 kHz regime. 120 kHz regime showed increase in radical generation

by 0.48, 0.55 and 0.97 % for Φ = 0.76 and 0.39, 0.47 and 0.62 % for Φ = 0.71, while energy consumption was 33.3 % and 30.2 % higher, compared to 80 kHz regime, respectively. Higher calorific value mixture showed better results; while it was hard to evaluated radical increase under Φ = 0.83 due to high rates of their luminosity. Investigation of the radical emissions under Φ = 0.76 and Φ = 0.71 showed, that OH* increased by 0.49 %, C_2* increased by 0.32 %, and CH* increased by 0.62 % for the 80 kHz regime for Φ = 0.76. For 120 kHz regime emission intensification was by 0.73, 0.20 and 0.46 % while energy consumption for the 120 kHz regime was 30.71 % higher. Φ = 0.71 showed that OH* increased by 0.33 %, C_2* increased by 0.21 %, and CH* increased by 0.58 % for the 80 kHz regime for Φ = 0.76. For 120 kHz regime emission intensification was by 0.60, 0.34 and 0.58 % while energy consumption for the 120 kHz regime was 30.37 % higher.

It was determined that the 80 kHz regime holds higher potential due to the maximal volumetric energy density that is being transferred from the power source to the gas. The highest volumetric density (both for $BG_{25/75}$ and $BG_{60/40}$) was observed for the 80 kHz regime, reaching 3.305 J/m^3 for $BG_{25/75}$ and 3.167 J/m^3 for $BG_{60/40}$. Compared with other peaks, for the $BG_{25/75}$ 80 kHz peak showed higher energy density at 26 %, 45 % and 53 % for 60 kHz, 100 kHz and 120 kHz regimes, respectively. For $BG_{60/40}$ the trend was similar, and the difference between volumetric energy density for 80 kHz discharge and 60 kHz, 100 kHz, and 120 kHz were 16 %, 51 % and 69 %, respectively. Assumed, that this happens due to variations in the average energy available per molecule in the plasma for activation and plasma-chemical reactions, both before and after reaching the dissociation energy of the C-O bond break in CO_2. After reaching this energy threshold, production rates of carbon-containing radicals (C_2 and CH) exhibit higher increases compared to the lighter OH radical.

The determined spatial emissions of OH*, C_2* and CH* indicate that with increasing plasma discharge frequency, the intensities in the flame are increase showing a positive influence on the combustion as low calorific value mixture ($BG_{25/75}$) becomes more stable and the flame chemiluminescence and shape corresponds to the higher calorific value gas ($BG_{60/40}$) without assistance. For $BG_{25/75}$, the decrease of the flame lift-off height was reduced by 2.43 %; 13.17 % and 3.33 % for the cases with Φ = 0.83, Φ = 0.76 and Φ = 0.71 respectively for the C_2* radical under plasma assistance. In general, the low calorific value mixture showed a good response to the plasma driving frequency (120 kHz) as the flame lift-off reduction was higher, being 16.34, 12.35 and 3.33 % for Φ = 0.83, Φ = 0.76 and Φ = 0.71 respectively.

Lower calorific value gas ($BG_{25/75}$) showed increasing rates of CO production while driving frequency was rising. Without plasma assistance Co emissions were registered at 3580, 2286 and 2456 ppm levels, but through the process of driving frequency increase, they raised to 6556, 5022 and 4066 ppm for the 80 kHz regime and to 7750, 5200 and 4966 ppm for 120 kHz regimes, for Φ = 0.83, Φ = 0.76 and Φ = 0.71 respectively. Meanwhile, the plasma-assisted combustion of the biogas mixture ($BG_{60/40}$) showed the significant impact of the flame stability by shifting the flame closer the burner cone. The flame lift-off height was reduced by 46.58, 51.28 and 46.3 % for Φ = 0.83, Φ = 0.76 and Φ = 0.71 respectively at 120 kHz regime. Besides it also led to increased combustion efficiency as CO emissions were 45, 46 and 210 ppm for Φ = 0.83, Φ = 0.76 and Φ = 0.71, respectively, at 120 kHz regime while CO emissions were high (700, 1537 and 2267 ppm, respectively, for Φ = 0.83, Φ = 0.76 and Φ = 0.71) under normal combustion conditions. Despite increased combustion efficiency, higher driving frequency regimes (120 kHz) negatively influenced nitrogen emissions in different oxide forms. That could be noted especially for higher calorific value gas, where NO_x emissions reached 450, 440 and 409 ppm for Φ = 0.83, Φ = 0.76 and Φ = 0.71, respectively, while plasma assistance was on, and plasma frequency was settled at 120 kHz. With unassisted combustion, NO_x emissions reached 25, 18 and 13 ppm, respectively, for the same air excess ratios. LCV gas showed the same trend, with NO_x emissions rising up from 6 ppm to 230, from 7 to 246, and from 33 to 264 ppm for Φ = 0.83, Φ = 0.76 and Φ = 0.71, respectively.

CRediT authorship contribution statement

Ernest Bykov: Writing – review & editing, Writing – original draft, Visualization, Validation, Resources, Methodology, Investigation, Formal analysis. **Adolfas Jančauskas:** Methodology, Investigation. **Rolandas Paulauskas:** Supervision, Conceptualization. **Kęstutis Zakarauskas:** Resources, Conceptualization. **Nerijus Striūgas:** Writing – review & editing.

Declaration of competing interest

The authors declare the following financial interests/personal relationships which may be considered as potential competing interests: [Rolandas Paulauskas reports financial support was provided by Research Council of Lithuania. If there are other authors, they declare that they have no known competing financial interests or personal relationships that could have appeared to influence the work reported in this paper].

Data availability

Data will be made available on request.

Acknowledgment

This project has received funding from the Research Council of Lithuania (LMTLT), agreement No S-MIP-23-116.

References

[1] Balances. AIWE. https://www.iea.org/data-and-statistics/data-tools/energy-statistics-data-browser?country=WORLD&fuel=Energy%20supply&indicator=TESbySource 2020.
[2] Kobayashi H, Hayakawa A, Somarathne KDKA, Okafor EC. Science and technology of ammonia combustion. Proceedings of the Combustion Institute 2019;37:109–33. https://doi.org/10.1016/j.proci.2018.09.029.
[3] Morlanés N, Katikaneni SP, Paglieri SN, Harale A, Solami B, Sarathy SM, et al. A technological roadmap to the ammonia energy economy: current state and missing technologies. Chem Eng J 2021:408. https://doi.org/10.1016/j.cej.2020.127310.
[4] Share of energy consumption from renewable sources in Europe https://www.eea.europa.eu/ims/share-of-energy-consumption-from 2022.
[5] Al Mamun MR, Torii S. Enhancement of methane concentration by removing contaminants from biogas mixtures using combined method of absorption and adsorption. Int J Chem Eng 2017;2017. https://doi.org/10.1155/2017/7906859.
[6] Sinigaglia T, Evaldo Freitag T, Machado A, Pedrozo VB, Rovai FF, Gondim Guilherme RT, et al. Current scenario and outlook for biogas and natural gas businesses in the mobility sector in Brazil. Int J Hydrogen Energy 2022;47:12074–95. https://doi.org/10.1016/j.ijhydene.2022.01.234.
[7] Bumharter C, Bolonio D, Amez I, García Martínez MJ, Ortega MF. New opportunities for the european biogas industry: a review on current installation development, production potentials and yield improvements for manure and agricultural waste mixtures. J Clean Prod 2023:388. https://doi.org/10.1016/j.jclepro.2023.135867.
[8] Bansal T, Tripathi N, Chawla G. ICGSEE-2013[14 th-16 th March 2013] International Conference on Global Scenario in Environment and Energy Upgradation Of Biogas Using Combined Method Of Alkaline Water Scrubbing And Adsoption Through Carbon Molecular Sieve. vol. 5. n.d.
[9] Paulauskas R, Skvorčinskienė R, Zakarauskas K, Striūgas N. Combustion performance of low calorific gas enriched by oxygen and ozone. Fuel 2022:324. https://doi.org/10.1016/j.fuel.2022.124761.
[10] Valipour Berenjestanaki A, Kawahara N, Tsuboi K, Tomita E. Performance, emissions and end-gas autoignition characteristics of PREMIER combustion in a pilot fuel-ignited dual-fuel biogas engine with various CO2 ratios. Fuel 2021:286. https://doi.org/10.1016/j.fuel.2020.119330.
[11] Peña Eguiluz R, López-Callejas R, González-Arciniega E, Rodríguez-Méndez BG, Mercado-Cabrera A, Guakil-Haber A, et al. Non-thermal plasma wound healing after removal of a neck tumor in a patient with HIV: a case report. Otolaryngology Case Reports 2022:22. https://doi.org/10.1016/j.xocr.2021.100391.
[12] Moridi Mahdieh Z, Shekarriz S, Afshar TF. Fabrication of antibacterial and self-cleaning polyester/cellulose fabric by corona air plasma via an eco-friendly approach. Clean Technol Environ Policy 2022;24:2143–59. https://doi.org/10.1007/s10098-022-02304-2.

[13] Anoop N, Sundaramurthy S, Jha JM, Chandrabalan S, Singh N, Verma J, et al. Plasma catalysis: a feasible solution for carbon dioxide valorization? Clean Technol Environ Policy 2021;23:2789–811. https://doi.org/10.1007/s10098-021-02203-y.
[14] Bauner D, Laestadius S, Iida N. Evolving technological systems for diesel engine emission control: balancing GHG and local emissions. Clean Technol Environ Policy 2009;11:339–65. https://doi.org/10.1007/s10098-008-0151-x.
[15] Zembi J, Cruccolini V, Mariani F, Scarcelli R, Battistoni M. Modeling of thermal and kinetic processes in non-equilibrium plasma ignition applied to a lean combustion engine. Appl Therm Eng 2021:197. https://doi.org/10.1016/j.applthermaleng.2021.117377.
[16] Starikovskaia SM, Kukaev EN, Kuksin AY, Nudnova MM, Starikovskii AY. Analysis of the spatial uniformity of the combustion of a gaseous mixture initiated by a nanosecond discharge. Combust Flame 2004;139:177–87. https://doi.org/10.1016/j.combustflame.2004.07.005.
[17] Patel R, van Oijen J, Dam N, Nijdam S. Low-temperature filamentary plasma for ignition-stabilized combustion. Combust Flame 2023:247. https://doi.org/10.1016/j.combustflame.2022.112501.
[18] Starik AM, Bezgin LV, Kopchenov VI, Loukhovitski BI, Sharipov AS, Titova NS. Numerical study of the enhancement of combustion performance in a scramjet combustor due to injection of electric-discharge-activated oxygen molecules. Plasma Sources Sci Technol 2013:22. https://doi.org/10.1088/0963-0252/22/6/065007.
[19] Hicks A, Norberg S, Shawcross P, Lempert WR, Rich JW, Adamovich IV. Singlet oxygen generation in a high pressure non-self-sustained electric discharge. J Phys D Appl Phys 2005;38:3812–24. https://doi.org/10.1088/0022-3727/38/20/007.
[20] Raizer YP, and JEAllen. Gas discharge physics. vol. Vol. 1. Springer; 1991.
[21] Zhu J, Ehn A, Gao J, Kong C, Aldén M, Salewski M, et al. Translational, rotational, vibrational and electron temperatures of a gliding arc discharge. Opt Express 2017;25:20243. https://doi.org/10.1364/oe.25.020243.
[22] Chen W, Jin D, Cui W, Huang S. Characteristics of gliding arc plasma and its application in swirl flame static instability control. Processes 2020:8. https://doi.org/10.3390/PR8060684.
[23] Liu Y, Tan J, Wan M, Yao X. OH*and cH*chemiluminescence characteristics in low swirl methane-air flames. AIP Adv 2020:10. https://doi.org/10.1063/5.0002660.
[24] Li T, Adamovich IV, Sutton JA. Effects of non-equilibrium plasmas on low-pressure, premixed flames. Part 1: cH* chemiluminescence, temperature, and OH. Combust Flame 2016;165:50–67. https://doi.org/10.1016/j.combustflame.2015.09.030.
[25] Zhu J, Sun Z, Li Z, Ehn A, Aldén M, Salewski M, et al. Dynamics, OH distributions and UV emission of a gliding arc at various flow-rates investigated by optical measurements. J Phys D Appl Phys 2014:47. https://doi.org/10.1088/0022-3727/47/29/295203.
[26] Kim W, Cohen J. Plasma-assisted combustor dynamics control at realistic gas turbine conditions. Combust Sci Technol 2021;193:869–88. https://doi.org/10.1080/00102202.2019.1676743.
[27] Tian Y, Zhu J, Sun M, Wang H, Huang Y, Feng R, et al. Enhancement of blowout limit in a mach 2.92 cavity-based scramjet combustor by a gliding arc discharge. Proc Combust Inst 2023;39:5697–705. https://doi.org/10.1016/j.proci.2022.07.101.
[28] Sun J, Wu H, Tang Y, Kong C, Li S. Blowout dynamics and plasma-assisted stabilization of premixed swirl flames under fuel pulsations. applications in energy and combustion. Science 2023:14. https://doi.org/10.1016/j.jaecs.2023.100122.
[29] Blanchard V, Roqué F, Scouflaire P, Laux CO, Ducruix S, Blanchard VP. Lean Flame Stabilization With Nanosecond Plasma Discharges in a Gas Turbine Model Combustor 2023:2023–102621. https://doi.org/10.1115/GT2023-102621i.
[30] Xiong Y, Schulz O, Bourquard C, Weilenmann M, Noiray N. Plasma enhanced auto-ignition in a sequential combustor. Proceedings of the Combustion Institute 2019;37:5587–94. https://doi.org/10.1016/j.proci.2018.08.031.
[31] Vignat G, Minesi N, Soundararajan PR, Durox D, Renaud A, Blanchard V, et al. Improvement of lean blow out performance of spray and premixed swirled flames using nanosecond repetitively pulsed discharges. Proceedings of the Combustion Institute, vol. 38, Elsevier Ltd; 2021, p. 6559–66. https://doi.org/10.1016/j.proci.2020.06.136.
[32] Kim GT, Yoo CS, Chung SH, Park J. Effects of non-thermal plasma on the lean blowout limits and CO/NOx emissions in swirl-stabilized turbulent lean-premixed flames of methane/air. Combust Flame 2020;212:403–14. https://doi.org/10.1016/j.combustflame.2019.11.024.
[33] Hoffmann S, Koch R, Org Bauer H-J. NUMERICAL INVESTIGATION OF THE LOW-SWIRL FLOW IN AN AERONAUTICAL COMBUSTOR WITH ANGULAR AIR SUPPLY. 2021.
[34] Saqib Akhtar M, Shahsavari M, Ghosh A, Wang B, Hussain Z, Rao Z. Effect of fuel reactivity on flame properties of a low-swirl burner. Exp Therm Fluid Sci 2023;142. https://doi.org/10.1016/j.expthermflusci.2022.110795.
[35] An Q, Kheirkhah S, Bergthorson J, Yun S, Hwang J, Lee WJ, et al. Flame stabilization mechanisms and shape transitions in a 3D printed, hydrogen enriched, methane/air low-swirl burner. Int J Hydrogen Energy 2021;46:14764–79. https://doi.org/10.1016/j.ijhydene.2021.01.112.
[36] Smith LKHES and PWC. Principle of Low-swirl Combustion and Technology Transfer History. The Gas Turbine Handbook. 3rd ed., Engineering Faculty Book Gallery; 2006.
[37] Xiao Y, Cao Z, Wang C. Flame stability limits of premixed low-swirl combustion. Adv Mech Eng 2018;10. https://doi.org/10.1177/1687814018790878.
[38] Cheng R, Levinsky H. Lean premixed burners. Lean Combustion: Technology and Control: Second Edition, Elsevier Inc.; 2016, p. 203–29. https://doi.org/10.1016/B978-0-12-804557-2.00006-7.
[39] Bykov E, Striūgas N, Paulauskas R. Emission spectroscopy of CH4/CO2 mixtures processed in a non-thermal plasma augmented burner. Catalysts 2022;12. https://doi.org/10.3390/catal12121540.
[40] Anaconda Python distribution platform https://www.anaconda.com/ 2023.
[41] Zhu J, Gao J, Ehn A, Aldén M, Larsson A, Kusano Y, et al. Spatiotemporally resolved characteristics of a gliding arc discharge in a turbulent air flow at atmospheric pressure. Phys Plasmas 2017;24. https://doi.org/10.1063/1.4974266.
[42] Fridman A. Plasma Chemistry. Cambridge University Press; 2008. https://doi.org/10.1017/CBO9780511546075.
[43] Bogaerts A, Wang W, Berthelot A, Guerra V. Modeling plasma-based CO2 conversion: crucial role of the dissociation cross section. Plasma Sources Sci Technol 2016;25. https://doi.org/10.1088/0963-0252/25/5/055016.
[44] Rusanov VD, Fridman AA, Sholin GV. The physics of a chemically active plasma with nonequilibrium vibrational excitation of molecules. Soviet Physics Uspekhi 1981;24:447–74. https://doi.org/10.1070/PU1981v024n06ABEH004884.
[45] Pushkarev AI, Zhu AM, Li XS, Sazonov RV. Methane conversion in low-temperature plasma. High Energ Chem 2009;43:156–62. https://doi.org/10.1134/S0018143909030023.
[46] Lapalme D, Seers P. Influence of CO2, CH4, and initial temperature on H2/CO laminar flame speed. Int J Hydrogen Energy 2014;39:3477–86. https://doi.org/10.1016/j.ijhydene.2013.12.109.
[47] Zhang H, He L, Yu J, Qi W, Chen G. Investigation of flame structure in plasma-assisted turbulent premixed methane-air flame. Plasma Science and Technology, vol. 20, Institute of Physics Publishing; 2018. https://doi.org/10.1088/2058-6272/aa9850.
[48] Qi D, Ying Y, Mei D, Tu X, Liu D. Soot characteristics from diffusion flames coupled with plasma. Fuel 2023;332. https://doi.org/10.1016/j.fuel.2022.126126.
[49] Tan YR, Zong Y, Salamanca M, Martin JW, Dreyer JAH, Akroyd J, et al. Investigation on the effect of Charge injection from non-thermal plasma on soot formation in Laminar coflow diffusion flame. Combust Sci Technol 2023. https://doi.org/10.1080/00102202.2023.2206521.
[50] Cha MS, Lee SM, Kim KT, Chung SH. Soot suppression by nonthermal plasma in coflow jet diffusion flames using a dielectric barrier discharge. Combust Flame 2005;141:438–47. https://doi.org/10.1016/j.combustflame.2005.02.002.
[51] Skvorčinskienė R, Striūgas N, Zakarauskas K, Paulauskas R. Combustion of waste gas in a low-swirl burner under syngas and oxygen enrichment. Fuel 2021;298. https://doi.org/10.1016/j.fuel.2021.120730.
[52] Striūgas N, Zakarauskas K, Paulauskas R, Skvorčinskienė R. Chemiluminescence-based characterization of tail biogas combustion stability under syngas and oxygen-enriched conditions. Exp Therm Fluid Sci 2020;116. https://doi.org/10.1016/j.expthermflusci.2020.110133.
[53] Feng R, Zhu J, Wang Z, Zhang F, Ban Y, Zhao G, et al. Suppression of combustion mode transitions in a hydrogen-fueled scramjet combustor by a multi-channel gliding arc plasma. Combust Flame 2022;237. https://doi.org/10.1016/j.combustflame.2021.111843.
[54] Snoeckx R, Bogaerts A. Plasma technology-a novel solution for CO2 conversion? Chem Soc Rev 2017;46:5805–63. https://doi.org/10.1039/c6cs00066e.
[55] Xu C, Tu X. Plasma-assisted methane conversion in an atmospheric pressure dielectric barrier discharge reactor. J Energy Chem 2013;22:420–5. https://doi.org/10.1016/S2095-4956(13)60055-8.
[56] Fathollahi P, Farahani M, Rad RH, Khani MR, Asadi A, Shafiei M, et al. Selective oxidation of methane to methanol by NTP plasma: the effect of power and oxygen on conversion and selectivity. J Electrostat 2021;112. https://doi.org/10.1016/j.elstat.2021.103594.
[57] Starik AM, Titova NS. Kinetics of detonation initiation in the supersonic flowof the H2 + O2 (air) mixture in O2 molecule excitationby resonance laser radiation. Kinet Catal 2003;44:28–39.
[58] Bak MS, Do H, Mungal MG, Cappelli MA. Plasma-assisted stabilization of laminar premixed methane/air flames around the lean flammability limit. Combust Flame 2012;159:3128–37. https://doi.org/10.1016/j.combustflame.2012.03.023.
[59] Barbosa S, Pilla G, Lacoste DA, Scouflaire P, Ducruix S, Laux CO, et al. Influence of nanosecond repetitively pulsed discharges on the stability of a swirled propane/air burner representative of an aeronautical combustor. Philosoph Trans Royal Soc A Mathem Phys Eng Sci 2015;373. https://doi.org/10.1098/rsta.2014.0335.
[60] Wu L, Fridman AA, Starikovskiy AY. Kinetics of Plasma Assisted Combustion At Low Reduced Electric Fields. n.d.
[61] Wang B, Chi Y. Kinetic study on high temperature oxidation of CO/H2/Cl 2 mixture. Proceedings - 2010 International Conference on Digital Manufacturing and Automation, ICDMA 2010, vol. 1, 2010, p. 886–91. https://doi.org/10.1109/ICDMA.2010.383.
[62] Paulauskas R, Skvorčinskienė R, Zakarauskas K, Striūgas N. Combustion performance of low calorific gas enriched by oxygen and ozone. Fuel 2022;324. https://doi.org/10.1016/j.fuel.2022.124761.
[63] Zhang H, Zhu F, Li X, Cen K, Du C, Tu X. Enhanced hydrogen production by methanol decomposition using a novel rotating gliding arc discharge plasma. RSC Adv 2016;6:12770–81. https://doi.org/10.1039/c5ra26343c.
[64] Tian X, Yang J, Gong Y, Guo Q, Wang X, Yu G. Experimental study on oH*, cH*, and CO2* chemiluminescence diagnosis of CH4/O2Diffusion flame with CO2-diluted fuel. ACS Omega 2022;7:41137–46. https://doi.org/10.1021/acsomega.2c04689.

[65] Sardeshmukh S, Bedard M, Anderson W. The use of oH* and cH* as heat release markers in combustion dynamics. Int J Spray Combust Dynam 2017;9:409–23. https://doi.org/10.1177/1756827717718483.
[66] García-Armingol T, Ballester J. Flame chemiluminescence in premixed combustion of hydrogen-enriched fuels. Int J Hydrogen Energy 2014;39:11299–307. https://doi.org/10.1016/j.ijhydene.2014.05.109.
[67] Oh S, Park Y, Seon G, Hwang W, Do H. Impacts of N2 and CO2 diluent gas composition on flame emission spectroscopy for fuel concentration measurements in flames. Int J Heat Mass Transf 2020;149. https://doi.org/10.1016/j.ijheatmasstransfer.2019.119174.